Chapter-5: Study of Structural-Electrical ……

5.1 Introduction

In previous chapter 4, it has been studied that how an alio-valent substitution with larger ionic radii than that of the host material at A-site enhance the ionic conductivity. Also, the tape of the composition, B1, among the series of investigated electrolyte systems was prepared. Preparing of the tape did not succeed due to improper optimization of binder, plasticizer defoaming agent, etc. and due to lack of proper instrumentation. Therefore, the tape casting technique has been left in this chapter and use pellets for further study instead of tape of the proposed system. Also, the tape casting technique has been left for future research work.

This chapter presents the investigation of double doped of an iso-valent substitution of Sm with smaller ionic radii on A-site of the co-doped LAO and the structural study of these samples has been carried out in detail and correlated with conductivity. Also, structural studies, the nature of transition, and the effect of the transition on the conductivity of prepared electrolyte systems are carried out in details.

5.2 Doping Strategy

As previously described in chapter 4 that the investigated system $(Sr_{0.1}La_{0.9})(Mg_{0.1}Al_{0.9})O_3$, i.e. B0, possesses better ionic conductivity than pure LAO. Effect of alio-valency on the system $(Sr_{0.1}La_{0.9})(Mg_{0.1}Al_{0.9})O_3$ with double substituted of Ba on La-site having larger ionic radii is also studied. It was concluded that larger ionic radii has increased the ionic conductivity for lower concentration of Ba. Now, It has been proposed an iso-valent double substitution of Sm with varying concentration of Sm i.e. $La_{0.9-x}Sr_{0.1}Sm_x\ Al_{0.9}Mg_{0.1}O_{3-\delta}$ where, x = 0.01, 0.03 and 0.05, and abbr. as S1, S3 and S5 respectively. Hence, the Goldschmidt tolerance [16] factor given in Eq. 1.14 has been

calculated for these sample (Fig. 5.1). It was found that the tolerance factor decreases with 'Sm' substitution and structure gets de-stabilize.

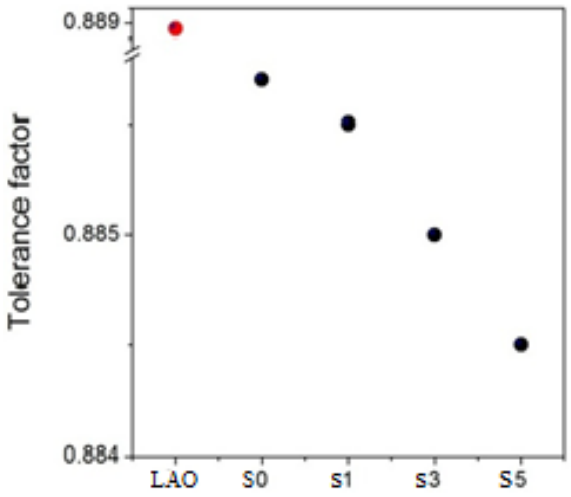

Figure 5.1: Tolerance factor of Sm substituted $La_{0.9}Sr_{0.1}Al_{0.9}Mg_{0.1}O_{3-\delta}$ (abbreviation: S0 for 0%, S1 for 1%, S3 for 3%, S5 for 5% substituted Sm, respectively and LAO for $LaAlO_3$)

The defect equations can estimate the number of oxygen vacancy generated with the substitutions and it can be written as (using Kroger -Vink notation):

$$xSm_2O_3 + 0.1SrO + 0.1MgO + xAl_2O_3 \xrightarrow{(0.1+2x)LaAlO_3} 0.1Sr'_{La} + 0.1Mg'_{Al} + 2xSm_{La} + 2xAl^{\times}_{Al} + (0.2+6x)O_O + 0.1\,V_O^{\bullet\bullet}$$

5.3 Experimental

The system $La_{0.9-x}Sr_{0.1}Sm_xAl_{0.9}Mg_{0.1}O_{3-\delta}$, (x = 0.00, 0.01, 0.03 and 0.05), LSSAM, and pure LAO were prepared by auto combustion synthesis using precursors and fuel. These precursors were weighed in appropriate stoichiometry to get desired composition. The details of synthesis process and characterization have been mentioned in chapter 2.

5.4 Results and Discussion

5.4.1 Phase Identification Using XRD

Figure. 5.2 (a) shows the XRD pattern of $La_{0.9-x}Sr_{0.1}Sm_x Al_{0.9}Mg_{0.1}O_{3-\delta}$, (x = 0.00, 0.01, 0.03 and 0.05), LSSAM, and pure LAO.

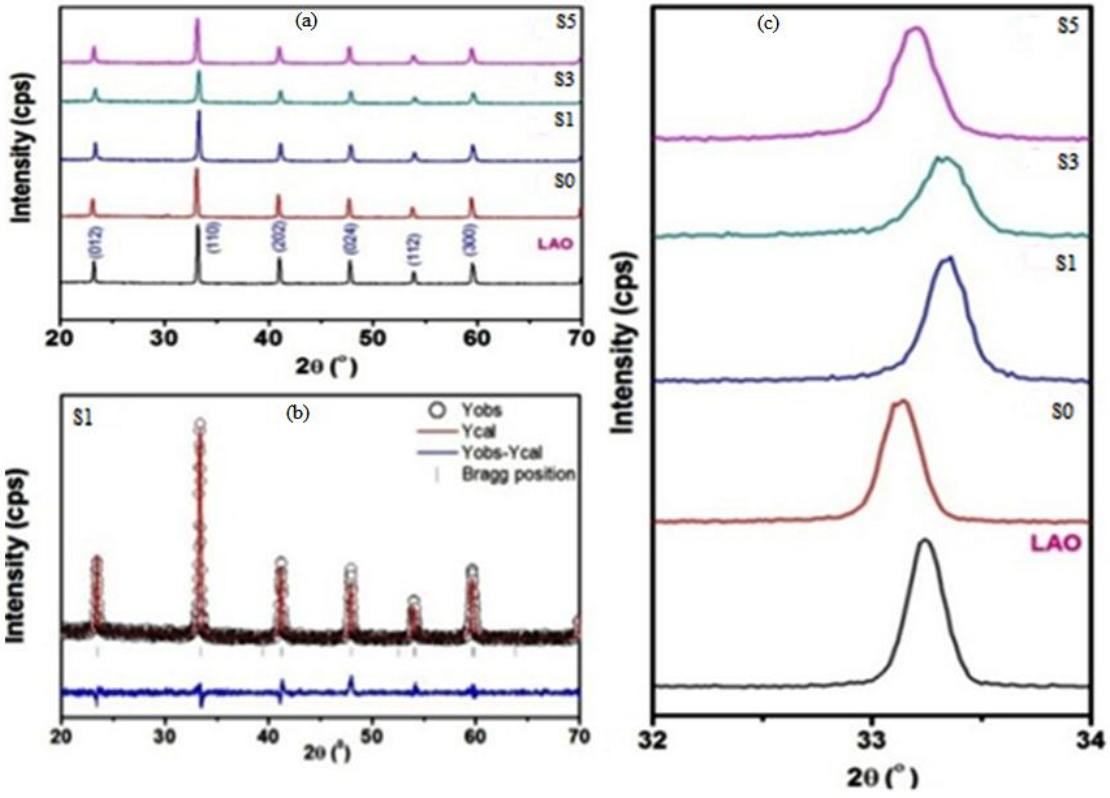

Figure 5.2: (a) XRD pattern of Sm substituted $La_{0.9}Sr_{0.1}Al_{0.9}Mg_{0.1}O_{3-\delta}$ **(b)** Reitveld refinement of S1 sample **(c)** shifting of (110) peak for LAO, S0, S1, S3 and S5 sample

The XRD pattern contains no impurity / secondary phase up to x = 0.05. The XRD peaks have been indexed on the basis of rhombohedral perovskite structure with space group R-3c using JCPDS file no. 82-0478 [32]. To check the symmetry, X-ray diffractograms have been refined using R-3c symmetry with Full Prof Suite software package. In the refinements, the peak shapes were described by pseudo-Voigt functions. For instance, Fig. 5.2 (b) depicts the calculated, observed and difference profiles of the S1 specimen obtained after Rietveld refinement and goodness of square fit obtained (χ^2) is 6.17. It has also been observed that the diffraction peaks slightly shift towards lower

angle with the substitution of Sr and Mg and towards higher angle with the 'Sm' substitution up to x = 0.03. With the further increase in 'Sm' substitution, the peak shifts towards lower angle again. To illustrate this, the peak (110) corresponding to $2\theta \approx 33^{o}$ is shown in Fig. 5.2 (c). The shift of diffraction peaks towards higher angle with increasing concentration of 'Sm' can be attributed to the smaller size of substituent ions like the ionic radius of Sm^{3+} (1.24 Å) is less than that of La^{+} (1.36 Å) [89].

5.4.2 Structural Analysis

The structure of the samples has been plotted using Diamond 3.0 software. The variation of lattice parameters, bond angle and bond length with respect to tolerance factor has been compared (Fig. 5.3 (a-b)). It has been observed that the lattice parameter 'a' and bond length Al-O increases for Sr and Mg substitution whereas decreases with the 'Sm' substitution and tolerance factor. Lattice parameter 'c' and Al-O-Al bond angle has shown a similar trend with tolerance factor.

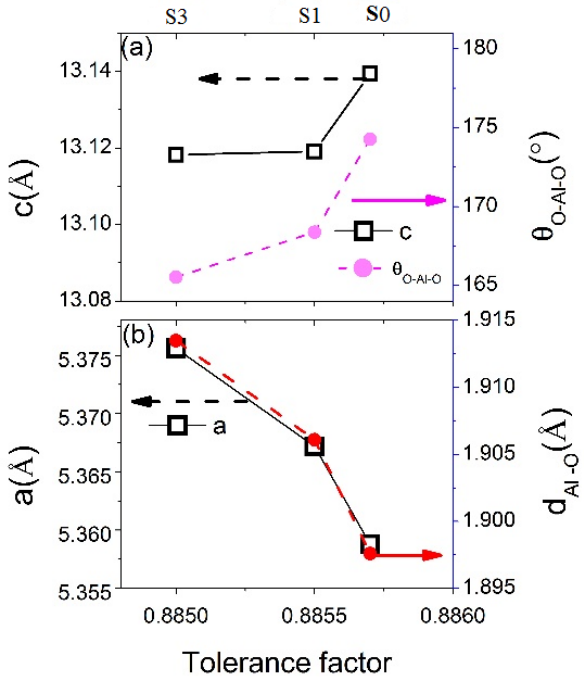

Figure 5.3: (a-b) Variation of Lattice parameters of Sm modified $La_{0.9}Sr_{0.1}Al_{0.9}Mg_{0.1}O_{3-\delta}$ (abbreviation: S0 or B0 for 0%, S1 for 1%, S3 for 3%, substituted Sm respectively and LAO for $LaAlO_3$) with tolerance factor

5.4.3 Compositional Details and Estimation of Oxygen Vacancy

Before the detail analysis of data, it was necessary to know about the elemental composition analysis of samples and its distribution. For this purpose, EDX has been carried out. The atomic % of Oxygen (Fig. 5.4) for various compositions has been estimated. We found that a deficiency of oxygen has been estimated and plotted in Fig. 5.4 (inset). The maximum deficiency is found for B0 sample. With the substitution of Sm, oxygen content has increased, but these samples (S0, S1, S3 and S5) are more oxygen deficient in comparison to pure LAO. Thus, there should be maximum oxygen vacancy for B0 sample and hence the ionic conductivity for B0. According to EDAX data, ionic conductivity decreases on increasing Sm concentration as like decrease in oxygen deficiency (S5 < S3 < S1).

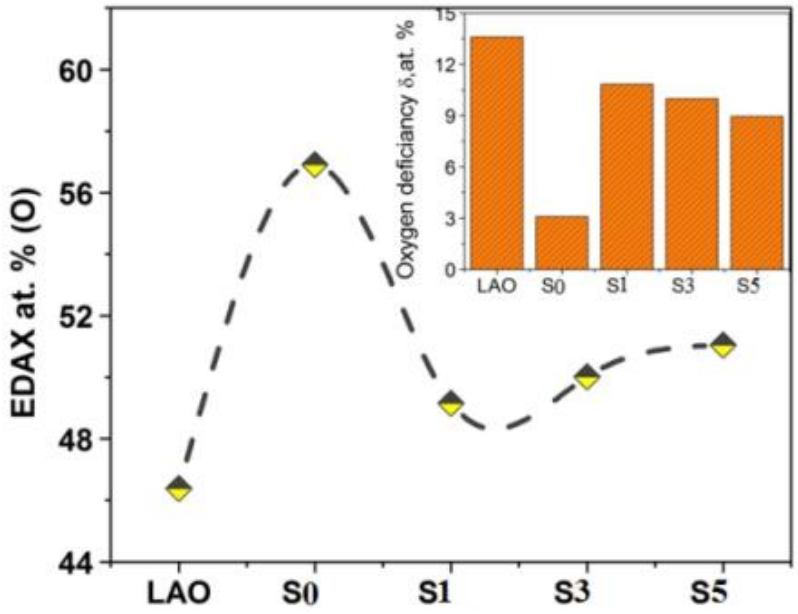

Figure 5.4: Oxygen estimated from EDX; inset: (right bottom) shows a deficiency of O in Sm modified $La_{0.9}Sr_{0.1}Al_{0.9}Mg_{0.1}O_{3-\delta}$(abbreviation: S0 for 0%, S1 for 1%, S3 for 3%, S5 for 5% substituted Sm respectively and LAO for LaAlO3)

5.5 Structure-Conductivity Correlation

As discussed earlier, in case of alio-valent substitution, critical triangle has played a major role in the transport of oxygen through it. In order to correlate conductivity with

the structure, the critical triangle study was further performed on a Sm substituted sample, i.e. an iso-valent substitution (as illustrated in Fig. 5.5). It has been observed that isosceles angle β (A-A-B/B-B-A) is in correlation to grain conductivity ($\sigma_g \approx \sigma_t$) and the vertex angle α (A-B-A/ B-A-B angle) is inversely correlated to dc conductivity (σ_0). Simultaneously, there is decrease in dc conductivity with the increase in 'Sm' content from S1 to S5 sample, while grain conductivity is slightly lower in S3 and S5 than tha of S1.

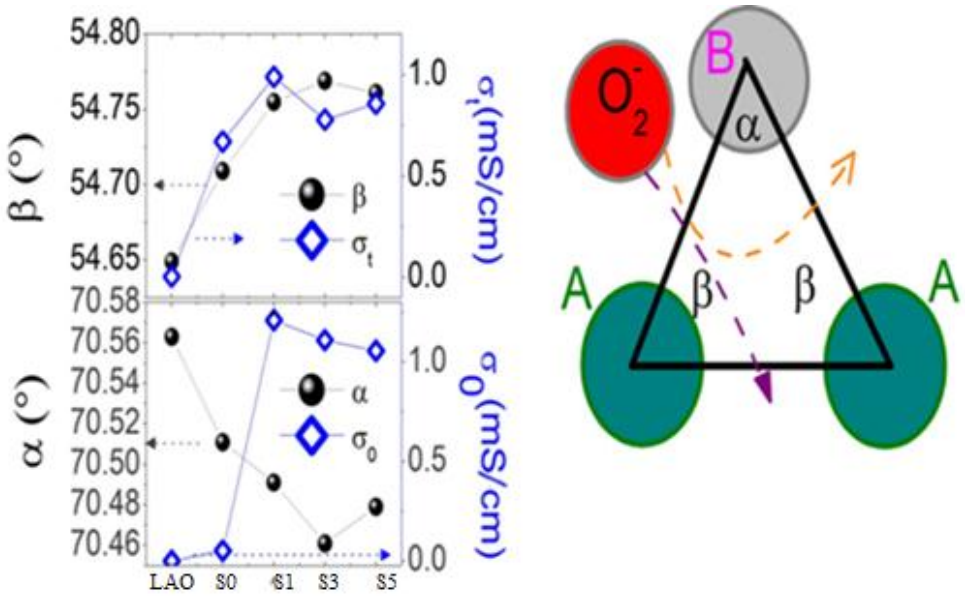

Figure 5.5: Correlation between the critical triangle structural parameter and the electrical parameters of Sm substituted $La_{0.9}Sr_{0.1}Al_{0.9}Mg_{0.1}O_{3-\delta}$(abbreviation: S0 for 0%, S1 for 1%, S3 for 3% and S5 for 5% substituted Sm respectively and LAO for $LaAlO_3$

The effect of substitution is clearly reflected in the results and can be understood as follows. The double substitution having small ionic radii and an iso-valent of Sm (only 1% by mole) at A-site of LSAM allows O_2^- to pass. With further substitution (just by 3% and 5% by mole), the value of grain conductivity decreases. When the conductivity is plotted with β, a similar trend is obtained with Sm substitution. That's why there is a correlation between β and grain conductivity.

Another critical triangle parameter is α angle. The small value of α, means greater intra-atomic interaction. In case of S0, where only La^{+3} is present at A-site, the correlation could not be established as La^{+3} does not have outermost shell (d) electron. Therefore, electronic conductivity is much reduced than expected from critical triangle analysis [28], [90]. The increase in dc conductivity for S1 is clearly due to maintain the charge neutrality. To maintain charge neutrality, only electron can commute through the critical triangle. This gives the possibility of polaronic conduction in Sm substituted samples [91].

The mechanism can be understood in terms of ionic radii (r_i) and length of sides of critical triangle (l_{ij}). The ionic radii of Sr, La and Sm with 12 co-ordination number are 1.44 Å, 1.36 Å and 1.09 Å [89]. It is well known that Sm ([Xe] $4f^6 6s^2$) Sr ([Kr] $5s^2$) are s-block element and s-electron has spherical electronic cloud. At B-site there is 'Al' and 'Mg' having Shannon ionic radii 0.535 Å and 0.72 Å respectively for VI co-ordination number [89]. It is well known that ionic radii of O_2^- is 1.4 Å with 6 co-ordination number. Now O_2^- to move through the critical triangle, it is necessary that $\Delta_{ij} \equiv l_{ij}-(r_i+r_j)$ should be greater than $2r_0$ (2.8 Å), where i,j is suffix for either of A, B. The value of $l_{AA} = l_{BB}$ is 3.7846 Å, 3.7905 Å, 3.7925 Å, 3.7964 Å and 3.7870 Å for LAO, S0, S1, S3 and S5, respectively. Now $\Delta_{BB} \approx \Delta_{AA} \approx 2.7964 \approx 2.8$ Å (detail calculation is given in chapter 4). Due to small ionic radii, bond length between AA, BB and AB (side of critical triangle) increases and thus, it is possible that O^{2-} can easily pass through the sides of critical triangle. As seen through EDAX graphs, in Sm substituted specimens, there is less oxygen deficiency. Hence, low oxygen vacancies will result in low ionic conductivity. To verify the ionic or electronic conductivity we have calculated transference number (T_f), which is ratio of ionic conductivity (σ_i) to total conductivity ($\sigma_i+\sigma_e$) [92], and found that Sm substituted system is second type ionic conductor ($0.3 < T_f < 0.8$) (Fig. 5.6, inset)

[93]. Hence due to an iso-valent substitution conductivity decreases on increasing Sm substitution shown in Fig. 5.6.

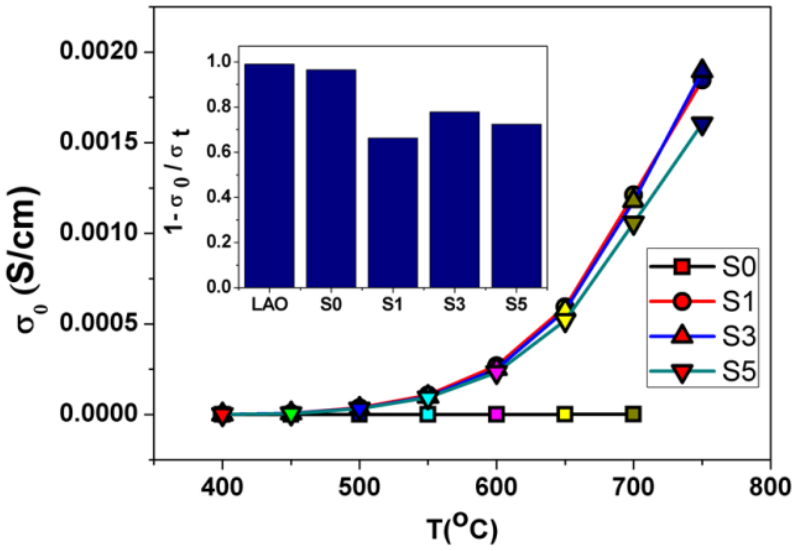

Figure 5.6: Variation of dc conductivity (σ_0) with temperature and transference number (T_f) with composition (inset)

5.6 Conductivity Spectroscopy and Differential Impedance Analysis

As discussed earlier, the only active ionic species is O_2^- ion and further the ionic conductivity at higher temperatures is directly related to the creation of oxygen vacancies in these substituted perovskite materials. It is observed in Fig. 5.6, that conductivity increases gradually after 500 ^oC. The above mentioned conductivity of these materials is analyzed using Jonscher Power law (Eq. 2.4) and impedance spectroscopy. For instance, the log-log plot of frequency dependence of ac conductivity at various temperatures for LAO and Sm substituted $La_{0.9}Sr_{0.1}Al_{0.9}Mg_{0.1}O_{3-\delta}$ (taken S1 sample) is shown in Fig. 5.7 (a) and Fig. 5.7 (b), respectively. From the fitting of data with the Jonscher Power law, dc conductivity (σ_{dc}), exponent (n) and hopping frequency (ν_H) have been calculated [86]–[88]. Further, various scaling tools have been followed to study the isotherms. Out of these tools, the conductivity spectra have been scaled using Hopping frequency as a scaling parameter known as Ghosh scaling (Eq. 2.6). Inset of Fig. 5.7 (a) depicts the

scaling isotherm for pure LAO that showing scaling is almost achieved in this sample. But with the substitution of Sr, Mg and different doping concentration of Sm, the scaling is achieved only for low temperature and low frequency, whereas the scaling is not achieved in high temperature and high frequency regime (Fig. 5.7 (c))

This depicts that there is change in conduction mechanism at high temperature i.e. qualitative change of charge carriers [94]. To verify the qualitative change of conduction mechanism, exponent has been plotted as a function of temperature for all the specimens. It is observed that in case of pure LAO, there is a minima at 400 ºC followed by an increase in the value of exponent with the increase in temperature showing the transformation from overlapping large polaron tunneling to small polaron hopping at 500 ºC [63]. Whereas, in case of Sr and Mg substituted specimen (S0), there is a continuous decrease in the value of exponent. The mechanism can be predicted on the basis of overlapping large polaron tunneling model. In case of S1 and S3, there is increase in the value of exponent upto 500 ºC, followed by a decrease in the value of exponent with the increase in temperature. In S1 and S3, there is a transition from small polaron to large polaron at 500 ºC.

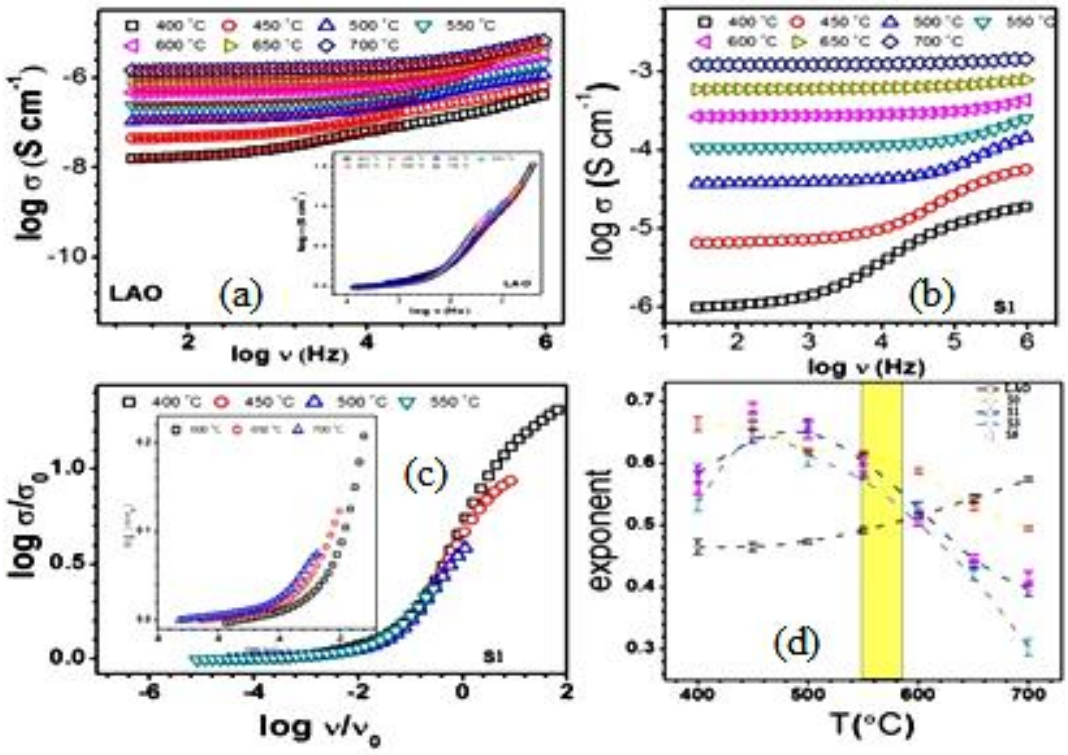

Figure 5.7: (a) logσ vs logν at various temperature for LAO (a inset) Ghosh scaling for LAO **(b)** logσ vs logν at various temperature for 0.01 mol % Sm substituted LAO (S1). Line indicate the fitting through J P law and symbol indicates data points **(c)** Ghosh scaling for S1 sample at low T (c inset) after 500 ºC **(d)** variation of n vs T

For further verification of the conduction mechanism and transition from large polaron hopping to small polaron hopping and vice versa, electrochemical behavior has been studied. Firstly, realization of equivalent circuits of Nyquist plots have been done. The Nyquist plots for the studied samples at 700 ºC are shown in Fig. 5.8. In pure LAO sample (Fig. 5.8 (a)), at 650 ºC it shows two semi- circular arcs in the low-frequency region and mid frequency region showing grain and grain- boundary contributions, respectively. Whereas, S0 sample (Fig. 5.8 (b)) shows, only one resistive grain, one semi-circular arc and a spike due to the electrode contribution. Fig. 5.8 (c-e) shows one resistive grain and two semi-circular arcs in the mid frequency region for S1 and S3 at 700 ºC, respectively. It is observed that with the increase in temperature a decrease in the value of resistance is observed. In order to correlate the electrical properties of the specimens with the microstructure of the sample, an equivalent circuit consisting of one

resistance and one parallel R-Q circuit connected in series has been used to interpret the nature of impedance plane plots with the help of Z-view software (inset of Fig. 5.8). Here R and Q are the resistance and constant phase element for the semi-circular contributions. It reveals non-ideal behavior of capacitance and occurrence of more than one relaxation processes with similar relaxation time.

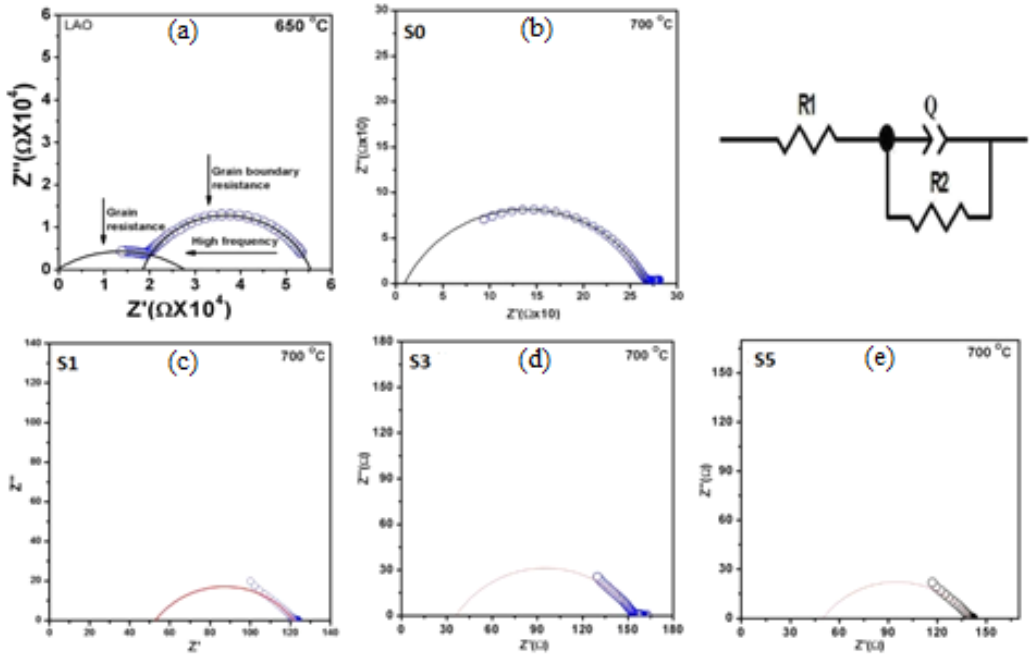

Figure 5.8 (a-e): Differential impedance of LAO and Sm substituted LSAM

The observation of constant phase element in the equivalent circuit confirms the distribution of charge carriers. Typically, for the distribution of charge carriers, high frequency data is required for measurement of fractal exponent (usually in the range of 0 to 1). Thus, according to the formalism of differential impedance analysis, value of fractal exponent has been calculated for the studied temperature range.

The capacitance of CPE is given by the relation $C = Q^{K}R^{(1-K)/K}$, where the parameter K estimates the deviation from ideal capacitive behavior [95]. The value of K is zero for the pure resistive case and unity for the pure capacitive one. The values of K are calculated from the slope of the corrected modulus, log|Z| vs log frequency plots

(Fig.5.9). Fig. 5.9 (a) and (b) shows the plot of log |Z| vs log frequency for S1 and LAO respectively. At higher frequencies, the corrected modulus is dominated by the contribution of the imaginary part of the impedance. The corrected modulus approaches zero according to $|Z|_{adj} \approx f^{K}$ [96]. Thus, the slope on a logarithmic plot has a value of –K at higher frequencies. It is observed that the value of K varies from 0.7 to 0.075 with corresponding increasing temperature from 400 ºC to 700 ºC in the studied samples (Fig. 5.9 (d)). In pure LAO, there is observed a dip at ~ 500 ºC, after which there is increase in the value of k with increasing temperature. Whereas in S0, S1 and S3, two transitions are observed in the region of 400 – 550 ºC, after which there is continuous decrease in the value of K with the increase in temperature. Usually, the value of K determines the roughness of the surface but the surface roughness gives only the minute changes. But in the present case, K changes with the temperature which can be attributed to the formation of ionic charge carriers in comparison to the deformation in the lattice [83], [96]. The variation of K with temperature in LAO is different from that of the substituted specimens. Variation of both the fractal exponent (K) and the exponent (n) with temperature shows change in relaxation mechanism in LAO and substituted specimens.

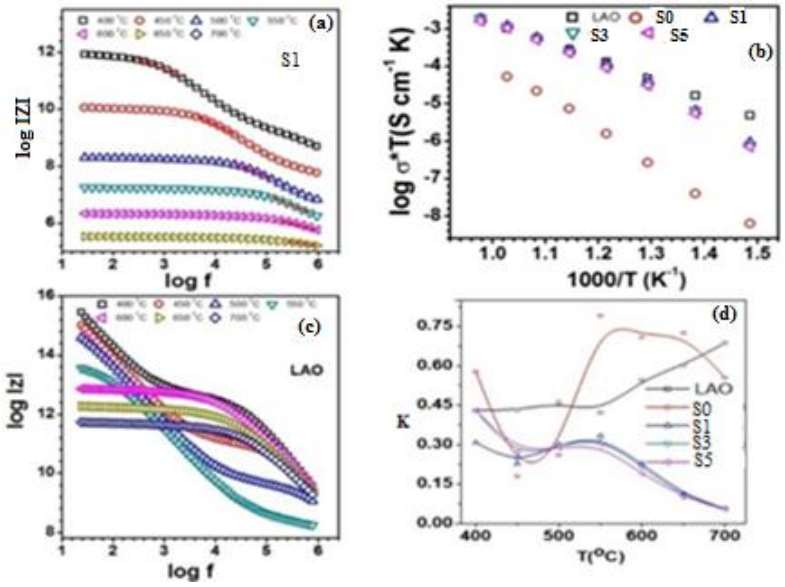

Figure 5.9: (a) log|z| vs log f of LAO and **(b)** Sm substituted LSAM, **(c)** activation energy curve **(d)** fractal exponent (k) vs temperature (°C)

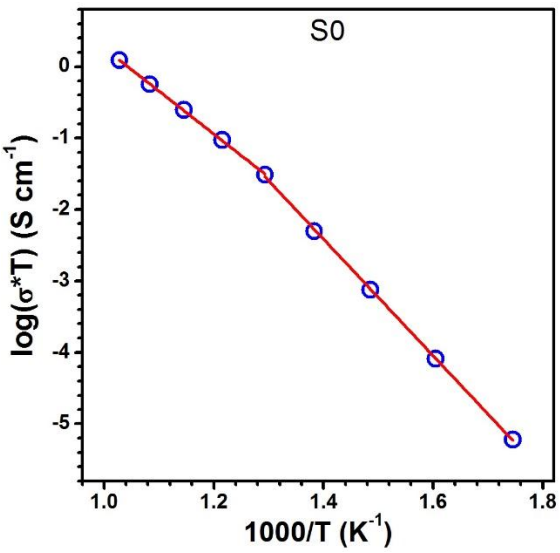

Figure 5.10: Activation energy curve for S0

As concluded from the exponent and fractal exponent graphs, there is a transition observed nearly at 500 ºC. This transition is also confirmed in the conductivity vs temperature plots where there is a sudden increase in the value of conductivity at ~500 ºC. From the scaling and exponent plots, a qualitative change in the charge carriers is confirmed. It is also observed the change in conduction mechanism from large polaron hopping to small polaron or vice versa with substitution. The activation energy has been estimated using conductivity calculated from Impedance spectroscopy i.e., 'σ_T'. Two slopes are observed from log (σT) vs 1000/T and in the range of 1-1.5 eV (Fig. 5.10) showing the formation of doubly ionized oxygen vacancies and the mechanism is oxygen vacancy assisted polaron conduction.

5.7 Microstructural Study

In order to relate the conversion from large polaron hopping to small polaron with temperature for LAO with the structure, hopping polaron length has been correlated with the lattice constants. It is well known that the size of the polarization cloud, called the coherence length, L_{coh}, is smaller than the unit cell dimension 'a', L_{coh} < 'a' the polaron

formed is a small polaron; the polaron formed is a large polaron if L_{coh} > a [97]. To analyze the formation of polarons, firstly 2(θ–δ) corresponding to XRD peak (110) of LAO where δ is the angle where maxima occurs (for instance) is plotted with temperature as shown in Fig. 5.11 (a). The observation of diffused intensity with the increase in temperature is showing the formation of polarons [98]. To find out the coherence length, microstrain and crystallite size has been calculated from HT-XRD results by using Williamson-Hall model. The Williamson Hall-model is given by Eq. 4.1 [82]. The slope of β cosθ vs 4sinθ curve (graphs not shown here) gives the value of microstrain and intercept gives the value of crystallite size. Fig. 5.11 (b) shows the value of microstrain and crystallite size. The values of microstrain and crystallite size showed the similar trend i.e. they are increasing with the increase in temperature up to 500 ºC and then decreases with the increase in temperature which indicates high amounts of strain with an amount of disorder in the system. To find out the coherence length, for spherical symmetry of grains, the coherence length depends on the crystallite size as one-third power of the crystallite size [99], $L_{coh}= t^{1/3}$. Fig. 5.11 (c) shows the variation of coherence length and crystallite size for LAO. It is observed that for pure LAO, the L_{coh} > c below 500 ºC shows the formation of large polarons. Whereas, for temperature above 500 ºC, L_{coh} < c (lattice constant) shows the formation of small polarons. This conversion is supporting the results obtained from fractal exponent (k) and exponent (n) behavior with temperature.

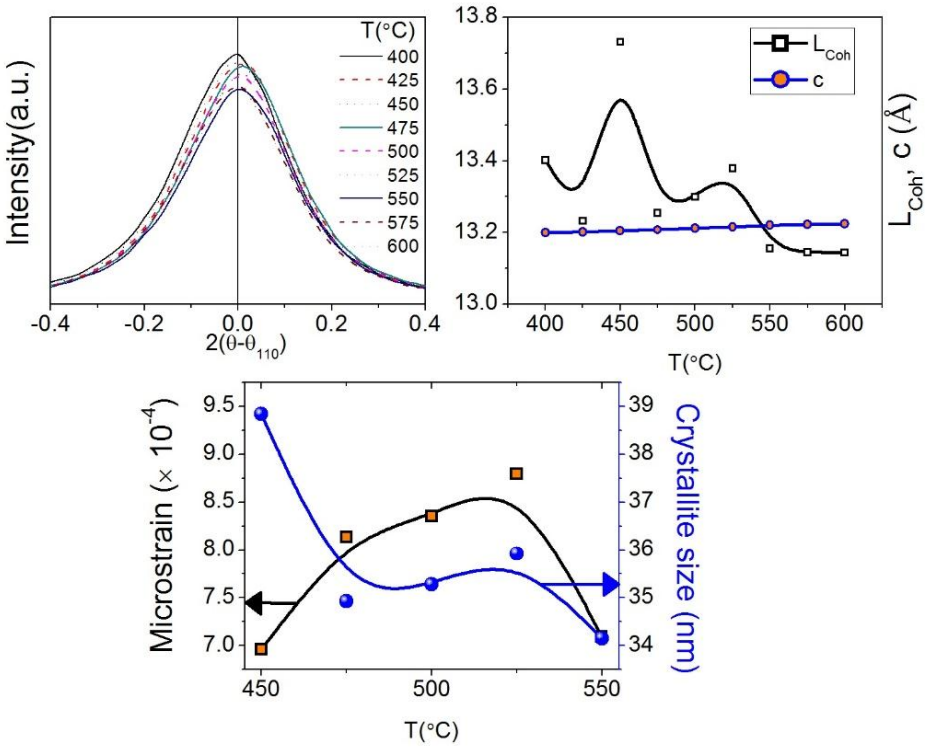

Figure 5.11 (a-c): Variation of microstructure with temperature for LSSAM sample

At nearly 500 ºC, a transition was confirmed with the help of impedance spectroscopy, differential impedance analysis and microstructural study.

The change in conduction mechanism is confirmed with the correlation of hopping polaron length with the lattice parameters. In the next step, the nature of the transition has been analysed, i.e. whether it is a phase transition or not.

5.8 Transition in LAO and Its Composition

In order to resolve this puzzle we performed high temperature XRD for base material LAO and one substituted system S0 (for instance) which is shown in Fig. 5.12 (a) and 5.12 (b). There is a single phase formation over all range of the temperature for both the samples. It shows thermally stable of the system. To resolve the ambiguity regarding phase transition, Rietveld analysis at every temperature for both the samples have been done using rhombohedral (R-3c) structure and cubic (pm-3m) structure.

Rietveld refinement of LAO and S0 at room temperature (for instance) is shown in Fig.5.13 (a-d). The value of χ^2 is minimum for R-3c structure but both are well refined.

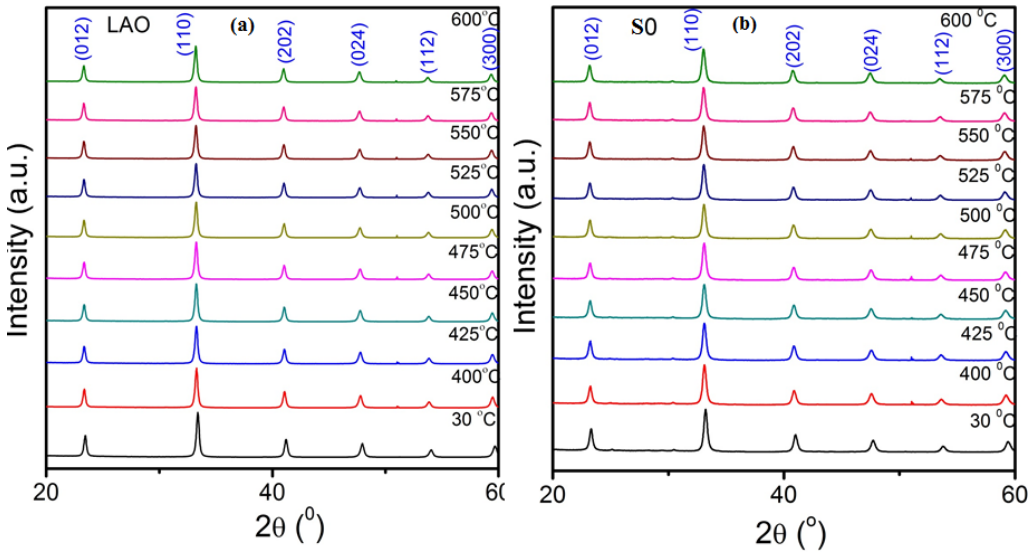

Figure 5.12: HT-XRD of LAO and S0

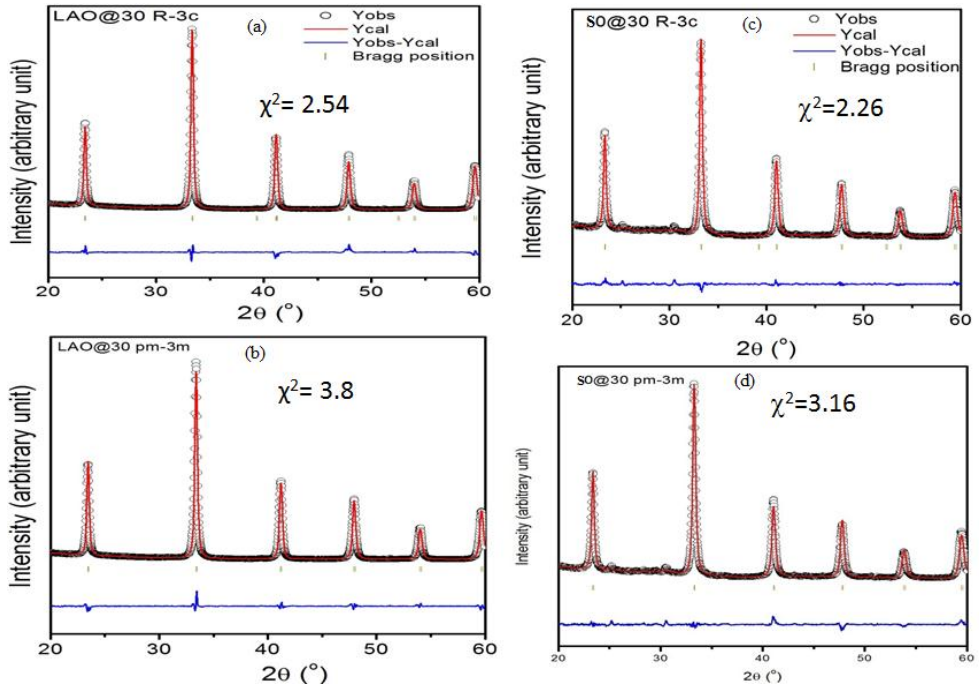

Figure 5.13: Rietveld refinement of LAO and S0 with R-3c and Pm-3m symmetry

For further analysis, we study the variation of bond angle (Fig. 5.14 (b)), obtained from Diamond software 3.0, with temperature and found that initially bond angle of LAO decreases to 160° at 475 °C and suddenly increased to nearly 180° at 500 °C and again

goes to nearly 169° at 600 °C. Similarly, for S0 sample bond angle reached to 180° at 525 °C and fall to 174° at 600 °C. Here at 500 °C structure gets stabilize to cubic and no tilting occurs in octahedron AlO_6. Since, bond angle and octahedral tilting are inversely correlated (Fig. 5.14 (a)). Also, there is same structure below and above the 500 °C which reveals LAO and its composition transform rhombohedral (R-3c) to pseudocubic (pm-3m) after at nearly 500 °C. This transition should be classified as phononic rather than structural transition [100]. At this temperature possibly due to triply degenerate R_{25} (R_{25} zone boundary phonon modes) soft phonon mode in which the adjacent octahedral along an axis vibrate about an axis in opposite senses which gives transition nearly at zone boundary known as zone boundary transition (ZBT) [101]–[103]. This R_{25} soft phonon mode involves rotations of the common structural element the AlO_6 octahedron of the perovskite structure [101]. R_{25} gives the rotation of the adjacent layers in opposite sense ($a^oa^oc^-$ in Glazer's notation). The soft mode remain underdamped, the damping constant of soft modes increased with temperature. Zone boundary transition (ZBT) is a single deriving mechanism, which increases conductivity after a zone boundary at a particular temperature [93], [100].

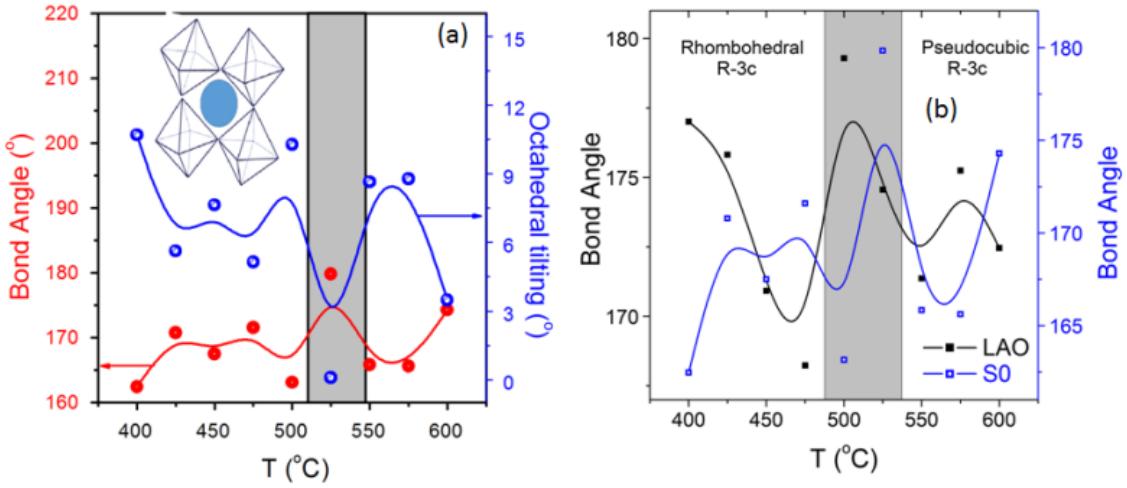

Figure 5.14: (a) Bond angle (^{0}) and tilting variation with temperature (°C) **(b)** Variation of bond angle with temperature (°C) For LAO and S0

In order to correlate this transition with the critical triangle, Fig. 5.15 shows the variation of critical triangle angle B-A-B (α) and A-B-B (β) with tilting angle (ϕ). At nearly 500 °C tilting of octahedron AlO_6 shows minimum value and below and above 500 °C it shows relatively high values. This indicates that cubic structure has stabilized at 500 °C (cubic) and below and above this temperature, it is rhombhohederal in structure. Also, after this temperature conductivity of LAO and its compositions increases suddenly to a high values. Hence zone boundary transition (ZBT) plays an important role to increase the conductivity in perovskite structure $LaAlO_3$.

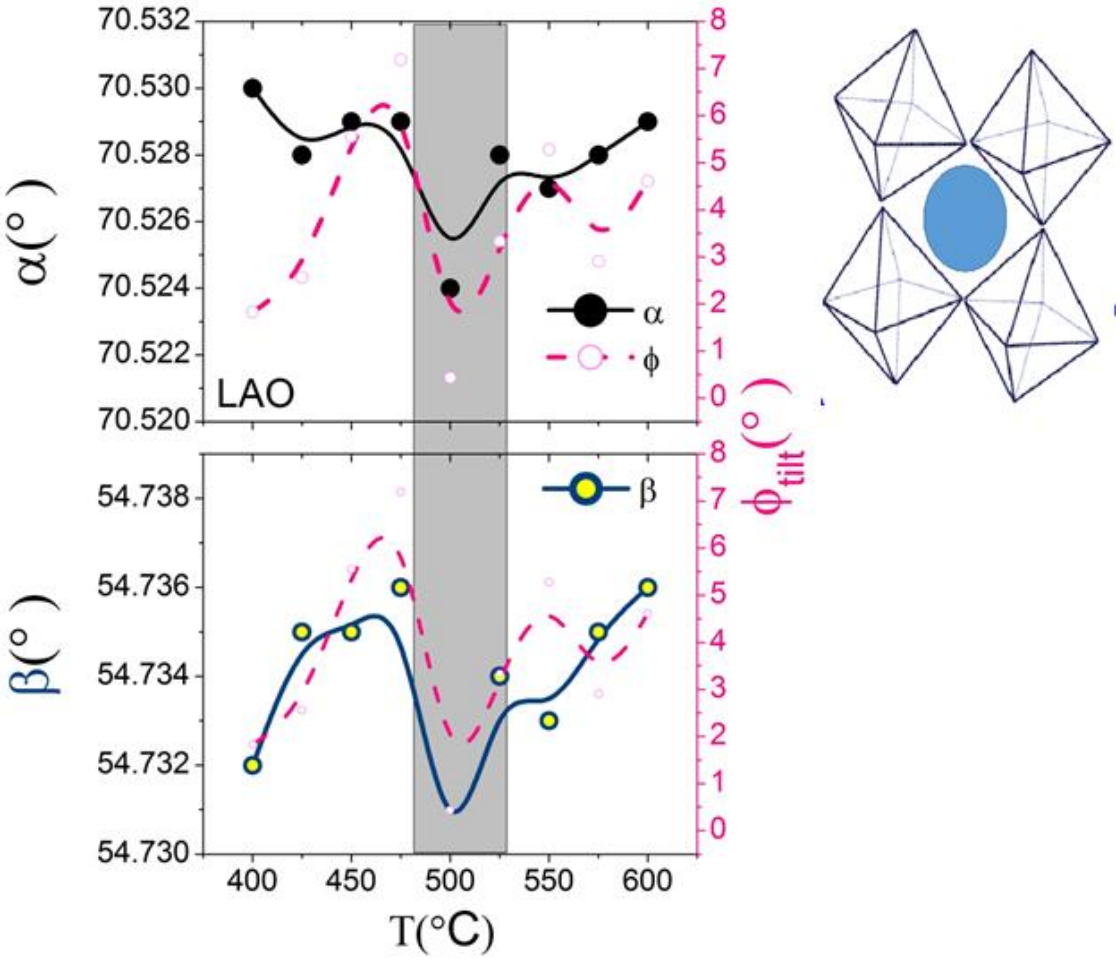

Figure 5.15: Variation of tilting with critical triangle angle B-A-B (α) and A-B-B (β)

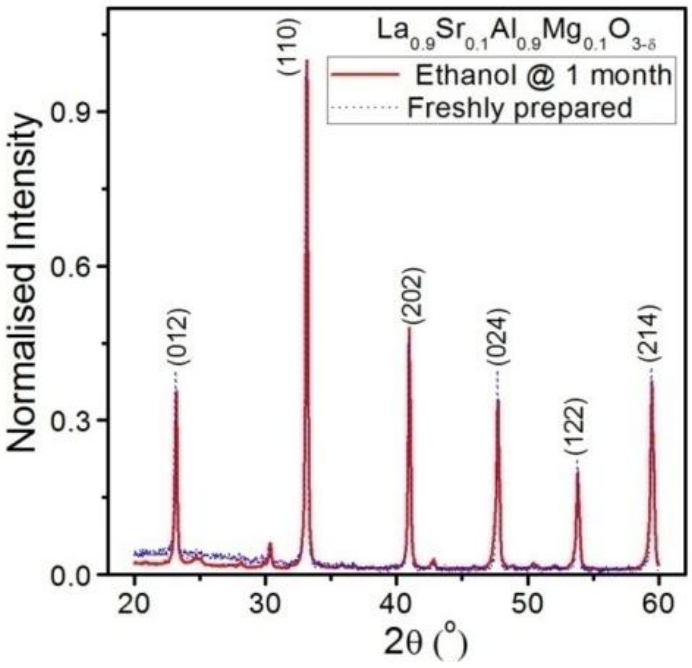

Figure 5.16: XRD pattern of S0 in inert atmosphere (dash line) and in ethanol dipped @ 1 month (solid line)

Since $LaAlO_3$ is thermally (Fig. 5.12) and chemically stable (Fig. 5.16). Also, it has high transference number (T_f) of 0.9 which shows high ionic conducting behavior and it has high density about nearly 95% (Archimedes principle). All the above results reveal that $LaAlO_3$ and its compositions is suitable candidate for electrolyte material of SOFC.

5.9 Conclusions

In summary, in Sm incorporated $La_{0.9}Sr_{0.1}Al_{0.9}Mg_{0.1}O_{3-\delta}$, it is found that with low ionic radii and high valence has decreased the ionic conductivity. On the basis of transference number (T_f) we can conclude that Sm substituted $La_{0.9}Sr_{0.1}Al_{0.9}Mg_{0.1}O_{3-\delta}$ have II type ionic. The conductivity of the investigated systems is in good correlation with critical triangle angle B-A-B (α) and A-B-B (β) as we have in seen earlier systems. Also, transition of investigated system from rhombohedral (R-3c) to pseudo cubic (R-3c) is due to zone boundary transition (ZBT) through R_{25} soft phonon mode at ~500 °C. This transition has been correlated with the octahedral tilting, as it is minimum at ~500 °C.

Also, critical triangle angles are found to possess minima at this temperature concluding this transition is not a phase transition rather it is a phonon mode transition. Hence, before and after 500 ºC it is rhombohedral in structure but this transition is useful for the electrolyte materials, as this has increased the conductivity.